Chemical Physics 518 (2019) 30–37

Contents lists available at ScienceDirect

Chemical Physics

journal homepage: www.elsevier.com/locate/chemphys

Key mechanistic details of paraoxon decomposition by polyoxometalates: Critical role of *para*-nitro substitution

Alexey L. Kaledin[a], Diego Troya[b], Christopher J. Karwacki[c], Alex Balboa[c], Wesley O. Gordon[c], John R. Morris[b], Mark B. Mitchell[d], Anatoly I. Frenkel[e,f], Craig L. Hill[g], Djamaladdin G. Musaev[a,g,*]

[a] Cherry L. Emerson Center for Scientific Computation, Emory University, Atlanta, GA 30322, USA
[b] Department of Chemistry, Virginia Tech, Blacksburg, VA 24061, USA
[c] U.S. Army Edgewood Chemical Biological Center APG, MD 21010, USA
[d] Department of Chemistry, Kennesaw State University, Kennesaw, GA 30144, USA
[e] Department of Materials Science and Chemical Engineering, Stony Brook University, Stony Brook, NY 11794, USA
[f] Department of Chemistry, Brookhaven National Laboratory, Upton, NY 11973, USA
[g] Department of Chemistry, Emory University, Atlanta, GA 30322, USA

ARTICLE INFO

Keywords:
Zirconium substituted polyoxometalates (POM)
Nerve agent simulant decomposition
Reaction mechanism
Critical role of *para*-nitro substitution
Water-splitting *vs* OH-transfer
Methyl-paraoxon

ABSTRACT

We report computational studies of (*O,O*-dimethyl)-(*O*-4-nitrophenyl)-phosphate (DMNP) and (*O,O*-dimethyl)-(*O*-phenyl)-phosphate (DMPP) decomposition by the Zr-substituted Polyoxometalate $\{\alpha\text{-}PW_{11}O_{39}Zr(\mu\text{-}OH)(H_2O)\}^{4-}$, which has been recently shown to be a catalytic active species in the reaction of $(Et_2NH_2)_8[\{\alpha\text{-}PW_{11}O_{39}Zr(\mu\text{-}OH)(H_2O)\}_2]\cdot 7H_2O$ with nerve agents. We studied two possible mechanisms of this reaction described as "*hydrolysis first*" and "*OH-transfer first*". Both reaction pathways are initiated from the same pre-reaction complex (H_2O)-(OH)-POM-(nerve agent). The "*hydrolysis first*" pathway starts by the concerted dissociation of the adsorbed water molecule and nucleophilic addition of the resulting OH group to the nerve agent. Conversely, the "*OH-transfer first*" pathway starts by nucleophilic addition of the Zr-coordinated OH ligand to the phosphorus of the nerve agent simulant. Calculations show that the "*OH-transfer first*" pathway exhibits a lower energy barrier for the decomposition of DMPP by ZrPOM. Thus, the presence of a hydroxo ligand in the coordination sphere of Zr(IV) introduces a mechanism switch from "*hydrolysis first*" [which was recently reported for the Sarin (GB) decomposition mechanism by the hexaniobate POM $Cs_8Nb_6O_{19}$] to "*OH-transfer first*". These findings imply that the pH of the catalytic solution could play a critical role and potentially control the mechanism of nerve agent and simulant decomposition by polyoxometalates. We also predict and corroborate that the presence of a strong electron-withdrawing *para*-substituent in the substrate phenyl group accelerates this reaction: DMNP decomposition by ZrPOM occurs with a smaller rate-limiting energy barrier. The calculations reveal several factors of the DMNP decomposition by the Zr(IV)-substituted polyoxometalates that provide design elements of Zr-based materials (including MOFs and POMs) for catalytic CWA decomposition under ambient conditions.

1. Introduction

Chemical warfare agents (CWAs) such as Sarin (GB), Soman (GD), methyl-Paraoxon (DMNP), Mustard (HD), and others (Scheme 1) present a threat to both the military and civilians [1–4], and constitute an increasing global risk. Therefore, the design of materials and technologies that can rapidly, and catalytically decompose CWAs is an active area of research [5–13]. It is apparent that an atomistic/molecular level understanding of catalytic CWA decomposition is critical for the development of effective catalysts for these processes. As such, previous studies [5,10] have established catalytic hydrolysis (both *specific* and *general* base hydrolysis, Scheme 2A) and oxidative (Scheme 2B) detoxification as possible mechanisms of the nerve and blister agent decomposition, respectively. Ongoing efforts have identified several enzymes (for example, acetylcholinesterase (a serine hydrolase)) [14], and organic and inorganic materials, including metal–organic frameworks (MOFs, especially UiO-66, NU-1000 and MOF-808) [9,15–30], polyoxometalates (POM) [31–35], MOF/POM hybrid materials

* Corresponding author.
E-mail address: dmusaev@emory.edu (D.G. Musaev).

https://doi.org/10.1016/j.chemphys.2018.11.013

Available online 19 November 2018

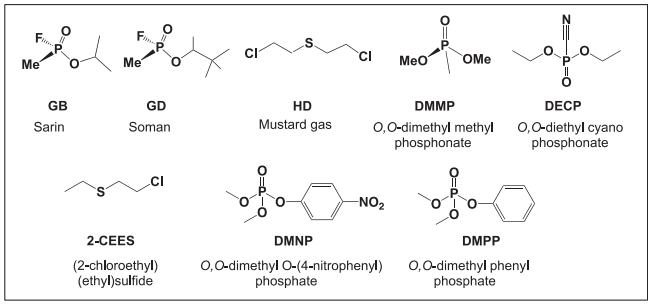

Scheme 1. Some of the extensively utilized chemical warfare agents (CWAs) and mimics pesticides. See also Ref. [4].

[36–39], zirconium hydroxide [40,41], zeolites [42,43], organic polymers [44], titania [45–47] as effective materials for decomposition of the organophosphorus (OP) nerve agents and pesticides.

Polyoxometalates (POMs) (Scheme 3) have long been of interest because they are molecular representations of metal oxides but far more amenable to extensive synthetic compositional alteration and characterization at the molecular level [48–61]. Their stability makes them broadly studied in various research domains, including materials science [52,54], medicine [53], and catalysis [50,51,55,59–61]. It is not surprising that they have also been identified as effective OP nerve agent hydrolysis compounds because their high negative charges can render them active players in nucleophilic processes.

In particular, Lindqvist polyoxoniobates (PONbs), a subset of POMs with six niobium centers, exhibit OP decomposition ability. [33,34,62,63] Therefore, the synthesis and in-depth analysis of structure and reactivity of various (alkali and organic) PONb salts have been subject of extensive studies.[62,63] These studies have shown that the structure and catalytic activity of these species depend on many factors including, but not limited to, the nature of counter-cation, solution pH, catalyst aggregate state, real-time environmental conditions, and the nature and concentration of ambient gas molecules. Our recent mechanistic studies [64] of OP decomposition by the cesium salt of hexaniobate, $Cs_8Nb_6O_{19}$, showed that reaction proceeds via a general base hydrolysis mechanism. We found that while the hydrolysis process is fast, a strong binding of product to the POM decreases its effectiveness and inhibits regeneration of the active catalyst. The calculations have revealed [65] that the presence of ambient gas molecules, such as CO_2 and SO_2, facilitates catalyst regeneration and could be helpful in making these processes truly catalytic.

Zirconium substituted polyoxometalates are another class of POMs and are also effective for CWA decomposition [56,57,58,66]. The presence of Zr(IV)-center(s) in the POM framework makes this class of molecular catalysts a tunable alternative to Zr-containing MOFs (such as UiO-66, NU-1000 and MOF-808) and zirconium hydroxides, both extensively studied for OP decomposition at the gas-surface interface. Consistent with these expectations, previous studies of the phosphoester bond hydrolysis in commonly used DNA models such as 4-nitrophenyl phosphate and bis-(4-nitrophenyl) phosphate by the POM $K_{15}H[Zr(\alpha_2\text{-}P_2W_{17}O_{61})_2]\cdot 25H_2O$ have provided promising results [67–77]. Inspired by these recent findings, we have recently studied dimethyl chlorophosphate (DMCP) and GB decomposition by $(Et_2NH_2)_8[\{\alpha\text{-}PW_{11}O_{39}Zr(\mu\text{-}OH)(H_2O)\}_2]\cdot 7H_2O$ (henceforth referred to as 2ZrPOM) by utilizing a multimodal approach involving X-ray absorption fine structure spectroscopy (XAFS), X-ray diffraction (XRD), Raman spectroscopy, diffuse reflectance infrared Fourier transform spectroscopy (DRIFTS), X-ray photoelectron spectroscopy (XPS) and density functional theory (DFT) calculations.[78] This multimodal approach enabled us to identify the nature of the catalyst *in operando* and also the decomposition products. We have shown that upon CWA (DMCP and GB) exposure, a 2ZrPOM-CWA adduct forms, and the 2ZrPOM dimer transforms to ZrPOM monomers with coordinatively unsaturated Zr(IV)-centers. The monomer species is proven to be the key catalytic intermediate.

Previously, we also have examined [79], under homogeneous conditions, the rates for hydrolysis of (*O,O*-dimethyl)-(*O*-4-nitrophenyl)-phosphate (DMNP or methyl-paraoxon) catalyzed by 2ZrPOM as a function of pH, ionic strength, catalyst, and substrate concentrations. For this purpose, the effect of acetate and phosphate buffers was examined. It was discovered that in this reaction acetate functions as a co-catalyst, but phosphate inhibits hydrolytic activity. Thus, the buffer anions play key roles in CWA hydrolyses either accelerating (co-catalyzing) or inhibiting the rate. DFT studies provided clear insight into distinct binding modes and associated energetics of these two buffer molecules. It was shown that $H_2PO_4^-$ binds directly to the Zr-center, which explains the loss of the nerve agent simulant hydrolysis activity in phosphate buffer. In contrast, with acetate, the zirconium center remains open to substrate binding as acetate binds in a non-competitive mode to the POM. The binding of acetate to the catalytically active zirconium likely provides a hydrolysis rate enhancement acting as a local base and/or shifting the dimerization equilibrium in favor of the more active monomer. This finding provides evidence that acetate-through-hydrogen bonding with water acts as a local base by facilitating the dissociation of H_2O into the OH^- nucleophile during reaction.

Inspired by the above developments, we herein conduct an in-depth study of the mechanism of the DMNP decomposition by 2ZrPOM. We use the monomeric species, ZrPOM, which bears OH and aqua ligands, as the active catalyst. From previous findings, a second water molecule is only weakly H-bonded to the key monomeric intermediate and does not contribute to the reaction outcome, thus it is excluded from the present work [78,79]. We study both (*O,O*-dimethyl)-(*O*-4-nitrophenyl)-phosphate (DMNP) and (*O,O*-dimethyl)-(*O*-phenyl)-phosphate (DMPP) decomposition by the ZrPOM (Scheme 1), and pay special attention to the impact of *para*-substitution in the phenyl group on the mechanism and the energetics of the studied reaction.

2. Computational details

The Gaussian 09 suite of programs [80] was used for all calculations. Geometry optimizations and frequency calculations for all reported structures were performed at the M06L level of density functional theory [81] and an ultrafine integration grid. Default convergence criteria were used throughout. We used the 6-31G(d) basis set for all main group elements and the Lanl2dz basis set with corresponding Hay-Wadt effective core potentials for Zr and W, as implemented in Gaussian09. Each reported minimum has all positive frequencies and each transition state (TS) structure has only one imaginary frequency. Intrinsic reaction coordinate (IRC) calculations were performed for transition state structures to confirm their identity. Bulk solvent effects are incorporated for all calculations (including the geometry optimization) using the self-consistent reaction field polarizable continuum model (IEF-PCM) [82] with water as the solvent. All reported enthalpies and Gibbs free energies, as $\Delta H/\Delta G$ in kcal/mol, are computed at 298.15 K and 1 atm.

3. Results and discussion

For sake of clarity, we discuss the mechanistic details only for the reaction of ZrPOM with DMPP. Later, we summarize our findings for the reaction of ZrPOM with DMNP, and briefly comment on the impact of *para*-nitro substitution on the reaction outcome.

Based on the well-established general base hydrolysis mechanism (Scheme 2A), the first step of the decomposition reaction is the nerve agent coordination to the coordinatively unsaturated Zr(IV)-center of the catalyst ZrPOM and the formation of the pre-reaction ZrPOM-DMPP complex (**R**) (Fig. 1). In this pre-reaction complex (**R**), there are several weak interactions between DMPP and the catalyst: (P=O^1)=Zr, (P=

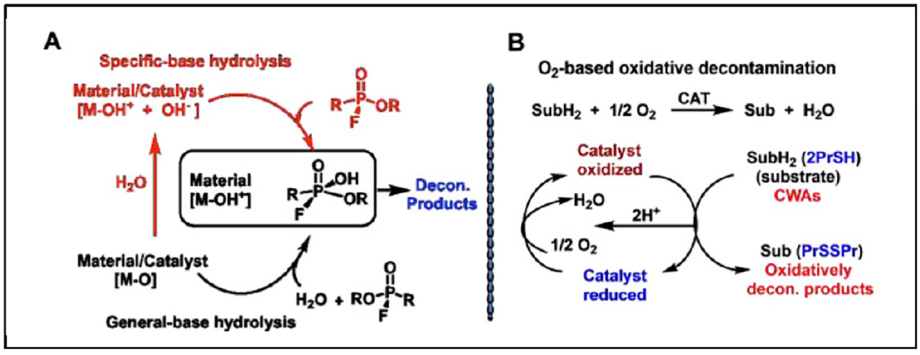

Scheme 2. (A) The established catalytic hydrolysis (both *specific* and *general* base), and (B) the oxidative detoxification mechanisms of nerve agent and blister agent decomposition, respectively.

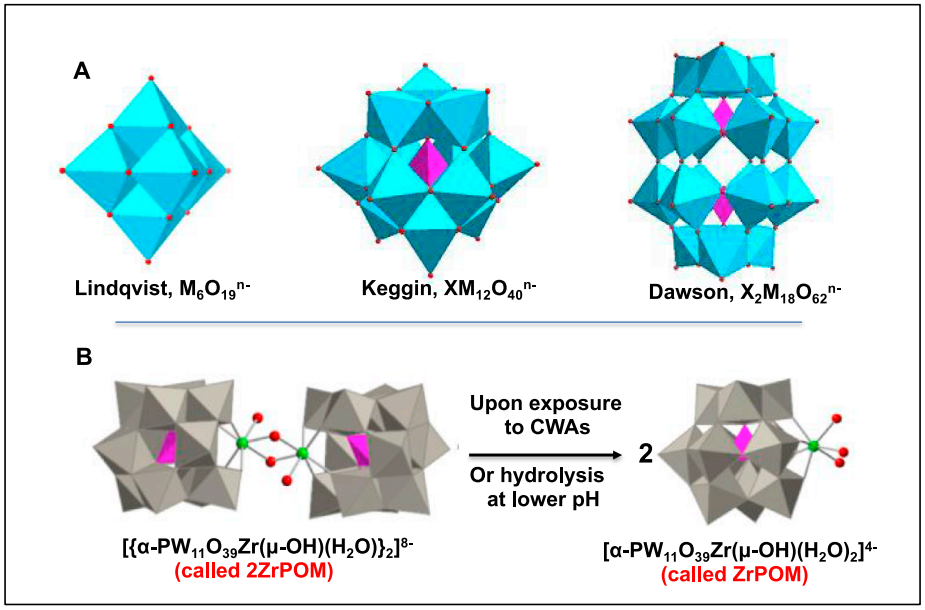

Scheme 3. (A) The most extensively utilized class of polyoxometalates: Lindqvist, Keggin and Dawson. Here, the blue octahedra are MO_6 units and the purple tetrahedra are internal XO_4 units; **(B)** The polyoxometalate $(Et_2NH_2)_8[\{\alpha\text{-}PW_{11}O_{39}Zr(\mu\text{-}OH)(H_2O)\}_2]\cdot 7H_2O$ 2ZrPOM) used in this paper. For simplicity, in our presentation the counter-cations and external water molecules are omitted. Code: WO_6, grey; PO_4, purple; Zr, green; and O red. (For interpretation of the references to colour in this figure legend, the reader is referred to the web version of this article.)

O^1)═H^1O^1 and (PO^4Me)═H^2OH^3 bonds have 2.459, 2.375 and 2.185 Å bond distances, respectively. These weak interactions of ZrPOM and DMPP in (**R**) are also manifested in a relatively small, ΔH = −17.7/G = −1.4 kcal/mol, complexation energy (i.e. energy of the ZrPOM + DMPP → (**R**) process). Note the H-bonding between the aqua ligand and bridging O^5-center of the catalyst: the calculated H^2OH^3═O^5 distance is 2.179 Å.

Previously, for the Sarin (GB) decomposition by the cesium salt of hexaniobate, $Cs_8Nb_6O_{19}$, we have established [64] that nerve agent decomposition initiated from an analogous **R** pre-reaction complex (H_2O)-POM-(nerve agent) is a multi-step process and proceeds via: (a) concerted dissociation of the adsorbed water molecule on a basic oxygen atom of the $Cs_8Nb_6O_{19}$ and nucleophilic addition of the OH group to the phosphorus center of the nerve agent, (b) rapid reorganization of the resulting pentacoordinated phosphorus intermediate, and (c) dissociation of the decomposition products and regeneration of the catalyst. Below, we call this the "*hydrolysis first*" mechanism.

However, the presence of OH-ligand at the Zr(IV)-center of ZrPOM makes it necessary also to investigate an alternative decomposition mechanism for DMPP (and DMNP) on ZrPOM, which can be initiated by the OH-ligand transfer from zirconium to the phosphorus of the nerve

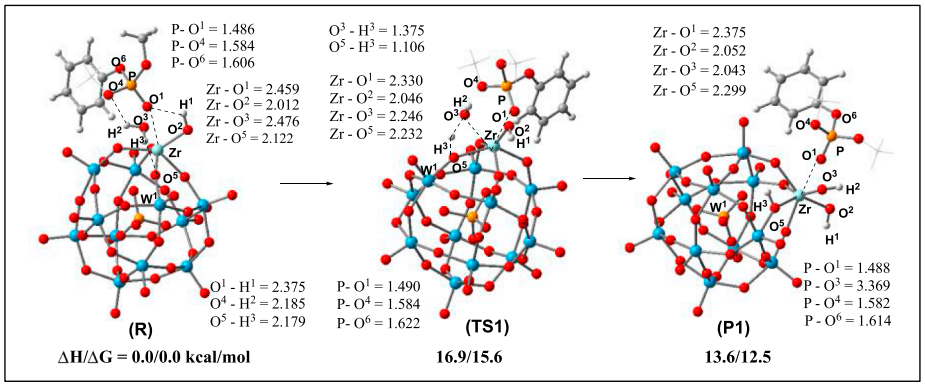

Fig. 1. Pre-reaction complex (**R**), hydrolysis transition state (**TS1**) and direct hydrolysis product (**P1**) of the reaction of ZrPOM with DMPP occurring via the "*hydrolysis first*" mechanism. Selected bond distances of these structures are given in Å, and their relative energies are presented in kcal/mol (see Supporting Materials for full structural parameters). Color code: W: blue, O: red, P: yellow, H: white, C: grey, Zr: light blue. (For interpretation of the references to colour in this figure legend, the reader is referred to the web version of this article.)

agent simulant and formation of the pentacoordinated phosphorus intermediate. From the resulted pentacoordinated phosphorus intermediate, reaction is expected to proceed via: (a) protonation of the either methoxy or phenol ligands of the OP species, and (b) dissociation of the decomposition products and regeneration of the catalyst. Below, we call this the "*OH-transfer first*" mechanism. Herein, in order to broaden applicability of outcomes of our studies (for the POM catalysts with and without hydroxo ligand), we investigate both "*hydrolysis first*" and "*OH-transfer first*" mechanisms for the DMPP and DMNP decomposition by ZrPOM.

The "Hydrolysis first" Pathway. We start our discussion with the "*hydrolysis first*" mechanism of DMPP decomposition on the ZrPOM. As we mentioned above, the first step after formation of the pre-reaction complex (**R**) is dissociation of the coordinated water molecule between the O^5- and Zr-centers of the polyoxometalate. At the corresponding hydrolysis transition state, (**TS1**), the broken O^3-H^3 bond is elongated to 1.375 Å, while the formed O^5–H^3 and Zr–O^3 bonds are 1.106 and 2.246 Å, respectively. The energy barrier associated with this water splitting step (calculated relative to the pre-reaction complex (**R**)) is 16.9/15.6 kcal/mol. Overcoming the barrier (**TS1**) leads to the metastable intermediate (**P1**), where the (POM)O^5–H^3 and Zr–O^3 bonds are fully formed. Since the intermediate (**P1**) lies 13.6/12.5 kcal/mol higher in energy than pre-reaction complex (**R**), it may easily rearrange to the latter.

Alternatively, the intermediate (**P1**) can undergo the Zr-to-P hydroxo transfer via a 5.4/9.7 kcal/mol energy barrier (relative to (**P1**)) at the transition state (**TS2**), and lead to the pentacoordinated phosphorus intermediate (**P2**) (Fig. 2). Overall, the (**R**) → (**P2**) transformation requires a 19.0/22.2 kcal/mol energy barrier and is uphill by 13.7/15.8 kcal/mol. In other words, the hydrolysis in the pre-reaction complex (**R**) is kinetically feasible but thermodynamically unfavorable. Therefore, the pre-reaction complex (**R**) can be considered as a resting state of the reaction.

From the high-energy hydrolysis intermediate (**P2**), the reaction of ZrPOM and DMPP may lead to the alcohol product formation via a proton transfer either to methoxy or phenoxy ligands of the phosphate. This is a very complex process, since potential source of proton could be either the previously oxidized POM fragment, the hydroxo ligand of the phosphate, or an adventitious water molecule.

Our calculations show that methanol formation occurs via proton transfer from the hydroxo ligand of the phosphate to the methoxy at the transition state (**TS3**). As seen in Fig. 3, at this transition state the activated O^3–H^2 and P–O^4 bonds are elongated to 1.352 and 1.815 Å, respectively, while the formation of the P–O^3 and O^4–H^2 bonds is initiated with lengths of 1.671 and 1.148 Å, respectively. Thus, this is a true OH-to-OMe proton-transfer transition state. While the resultant complex (**P3**) is 6.0/6.5 kcal/mol lower in energy than pre-reaction

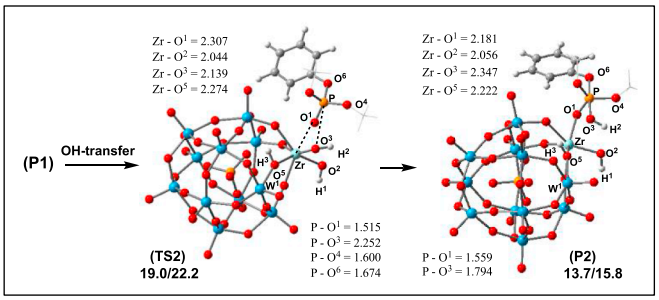

Fig. 2. The calculated OH-transfer transition state (**TS2**) and five-coordinated phosphorus product (**P2**) of the reaction of ZrPOM with DMPP occurring via the "*hydrolysis first*" mechanism. Selected bond distances of these structures are given in Å, while their relative energies are presented in kcal/mol (see Supporting Materials for full structural parameters). Same color code as Fig. 1. (For interpretation of the references to colour in this figure legend, the reader is referred to the web version of this article.)

complex (**R**), the calculated large, 43.5/44.9 kcal/mol, energy barrier makes methanol formation upon reaction of ZrPOM with DMPP exceedingly slow. The following, fast, proton (H^3) transfer from the O^5H^3-fragment of the POM to the just formed O^3(PO^3)-center completes the reaction and brings the intermediate (**P3**) and product complex (**P4**) to an equilibrium. The product complex (**P4**) with a weakly coordinated methanol and *O*-(methyl)-*O*-(phenyl)-(*O*-hydrogen)-phosphate (MPHP) is only 3.9/5.3 kcal/mol lower than the pre-reaction complex (**R**). The subsequent dissociation of methanol and MPHP ligands and coordination of water molecule complete the catalytic cycle.

Alternatively, from the same intermediate (**P2**), the reaction of ZrPOM with DMPP can proceed via phenol formation, which is found to occur via the hydroxo-to-phenoxy proton transfer transition state (**TS4**), with a notably smaller, 29.5/30.1 kcal/mol, energy barrier (calculated from the pre-reaction complex (**R**)). Close examination of (**TS4**) shows that it is a phenoxy dissociation-then-proton-abstraction transition state. Indeed, at this transition state the P—OPh bond is significantly elongated (to 2.228 Å), while the activated O—H bond is only slightly elongated (to 0.999 Å). A normal mode analysis of the reaction coordinate at **TS4** supports this conclusion (Fig. 4).

Overcoming this transition state leads to the intermediate (**P5**) with the weakly coordinated phenol and bidentate-coordinated dimethyl ester of phosphoric acid ligands, which is 10.7/10.2 kcal/mol lower than the initial complex (**R**). In this **P5** intermediate, similar to the methanol formation pathway, a rapid proton (H^3) transfer from the O^5H^3-fragment of POM to the newly formed O^3(PO^3)-center leads to the product complex (**P6**), which lies 13.7/12.1 kcal/mol lower than the initial complex (**R**). The product complex (**P6**) features weakly coordinated phenol and (*O,O*-dimethyl)-(*O*-hydrogen)-phosphate (DMHP) ligands, dissociation of which completes the catalytic cycle with coordination of a water molecule. One should note that the involvement of external water molecules into the proton shuttling between P-OH and methoxy and phenoxy groups could slightly reduce this energy barrier, but will not alter our conclusion.

In summary, the above presented discussion (also see Fig. 5, showing the reaction energy profile) unambiguously demonstrates that DMPP decomposition by the ZrPOM catalyst, via the "*hydrolysis-first*" mechanism, can lead only to phenol and (*O,O*-dimethyl)-(*O*-hydrogen)-phosphate (DMHP) products. Methanol and *O*-(methyl)-*O*-(phenyl)-(*O*-hydrogen)-phosphate (MPHP) formation requires a higher energy barrier and likely does not compete under ambient conditions. However, even phenol and DMHP formation requires an elevated (i.e. 29.5/30.1 kcal/mol) energy barrier in this mechanism. These findings suggest that timely decomposition of DMPP by ZrPOM via the "*hydrolysis-first*" mechanism may require harsh reaction conditions. Since the presented "*hydrolysis-first*" mechanism is, as previously was reported [64], the main decomposition mechanism of Sarin (GB) by the Lindqvist hexaniobate salts (for example, $Cs_8Nb_6O_{19}$), here we predict that the above presented findings are also applicable for the DMPP decomposition by the hexaniobate salts.

The "OH-transfer first" pathway. As mentioned above, the presence of a Zr-coordinated OH-ligand in the ZrPOM creates the possibility for an alternative DMPP decomposition mechanism initiated by the OH-transfer to the phosphorus center of the coordinated nerve agent simulant. The presented calculations show that this process occurs via the transition state **TS1a** (here and below, "**a**" in the labels of transition states, intermediates and products indicates the alternative, *OH-transfer first* pathway) with 11.3/12.3 kcal/mol energy barrier and leads to the pentacoordinated phosphorus intermediate (**P2a**). The OH-transfer process, i.e. (**R**) → (**P2a**), is found to be 5.9/5.8 kcal/mol thermodynamically uphill (see Fig. 6). Comparison of the calculated energetics for the initial steps of the "*OH-transfer first*" mechanism with those for the above-presented "*hydrolysis first*" pathway shows that the former process requires a smaller energy barrier (11.3/12.3 kcal/mol *vs* 19.0/22.2 kcal/mol) and is less endothermic (5.9/5.8 kcal/mol *vs* 13.7/15.8 kcal/mol). Therefore, the OH-transfer from zirconium to

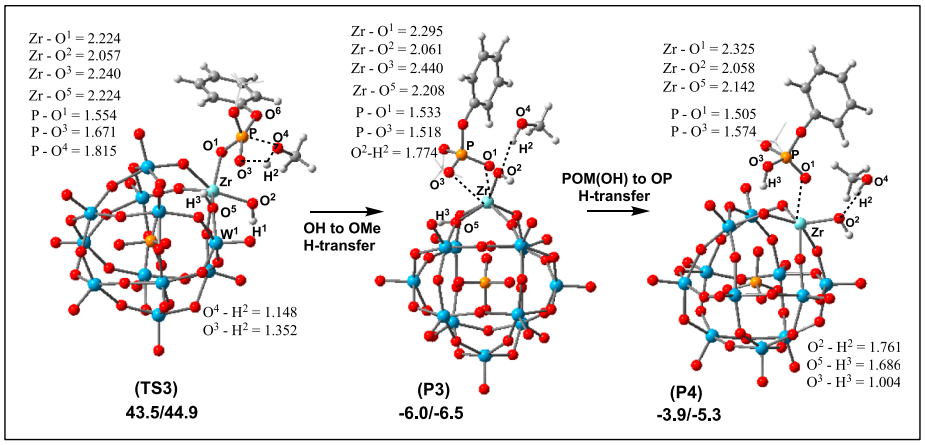

Fig. 3. The OH-to-OMe proton transfer transition state (**TS3**), direct product (**P3**) of this step, and product (**P4**) of the following proton transfer from the POM to the PO-unit. Selected bond distances of these structures are given in Å, while their relative energies are presented in kcal/mol (see Supporting Materials for full structural parameters). Same color code as Fig. 1. (For interpretation of the references to colour in this figure legend, the reader is referred to the web version of this article.)

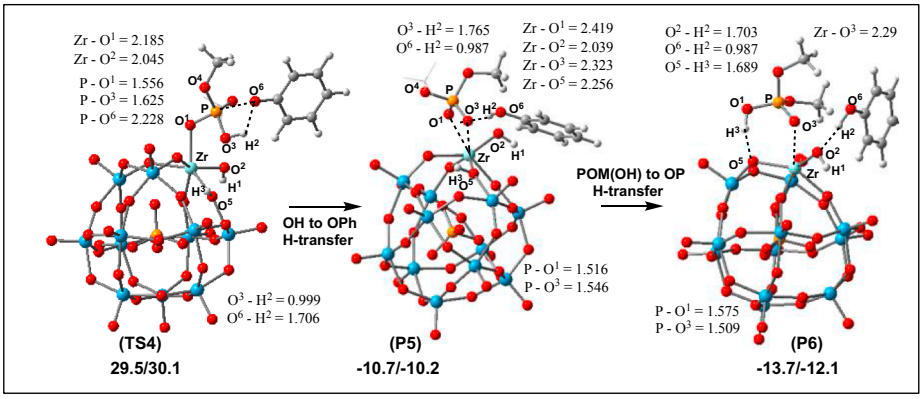

Fig. 4. The calculated OH-to-OPh proton transfer transition state (**TS4**), direct product (**P5**) of this process, and product (**P6**) of the following proton transfer from POM to PO-unit. Selected bond distances of these structures are given in Å, while their relative energies are presented in kcal/mol (see Supporting Materials for full structural parameters). Same color code as Fig. 1. (For interpretation of the references to colour in this figure legend, the reader is referred to the web version of this article.)

phosphorus in the pre-reaction complex (**R**) is expected to be the initial step of the DMPP decomposition by ZrPOM. However, this step of the reaction is energetically uphill and therefore the pre-reaction complex (**R**) remains the resting stage of the DMPP decomposition.

Interestingly, as seen in Figs. 2 and 6, the calculated pentacoordinated phosphorus intermediates of the "*hydrolysis first*" and "*OH-transfer first*" pathways, i.e. (**P2**) and (**P2a**) respectively, are related: intermediate (**P2**) converges to (**P2a**) by proton transfer from the POM-moiety to the Zr-coordinated OH-ligand. This process is thermodynamically favourable by 7.7/6.7 kcal/mol. However, for POMs with highly basic oxygen centers, like hexaniobates, one may expect the (**P2**) → (**P2a**) transformation will be thermodynamically unfavorable.

From the intermediate (**P2a**) the reaction may proceed to either methanol or phenol formation and associated *O*-(methyl)-*O*-(phenyl)-(*O*-hydrogen)-phosphate (MPHP) and (*O,O*-dimethyl)-(*O*-hydrogen)-phosphate (DMHP) decomposition products, respectively. However,

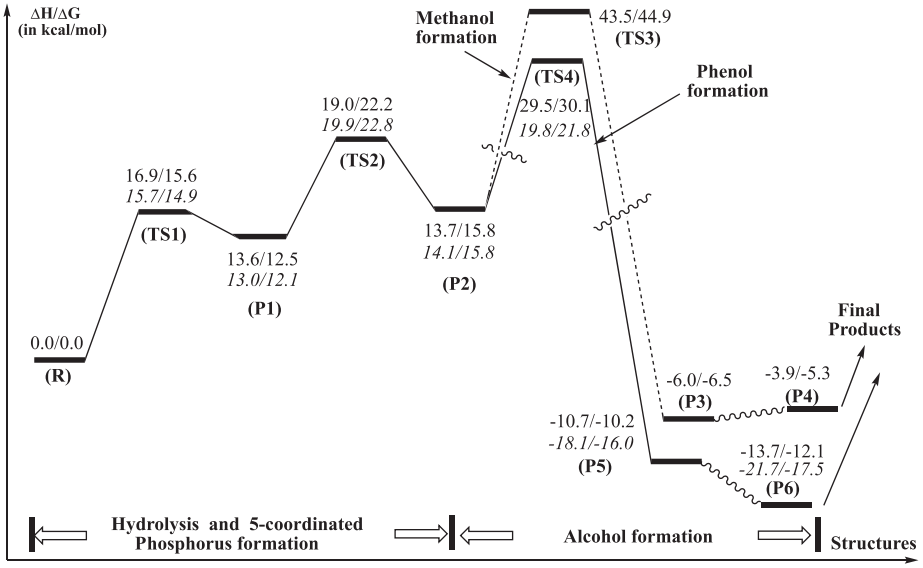

Fig. 5. The calculated energy surface (unscaled) of the reaction of ZrPOM with DMPP (regular numbers) and DMNP (italic numbers) proceeding via the "*hydrolysis first*" mechanism.

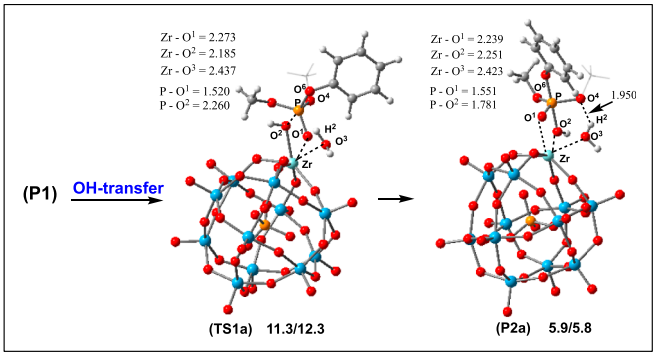

Fig. 6. The calculated OH-transfer transition state (**TS1a**) and intermediate (**P2a**). Selected bond distances of these structures are given in Å, while their relative energies (relative to pre-reaction complex (**R**)) are presented in kcal/mol (see Supporting Materials for full structure parameters). Same color code as Fig. 1. (For interpretation of the references to colour in this figure legend, the reader is referred to the web version of this article.)

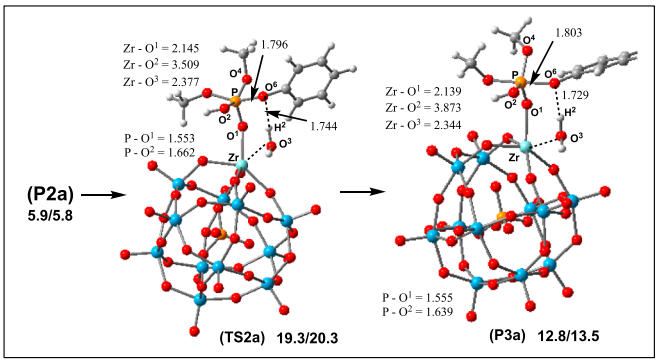

Fig. 7. The calculated Berry pseudorotation transition state (**TS2a**) and product (**P3a**) leading to phenol formation. Selected bond distances of these structures are given in Å, while their relative energies (relative to pre-reaction complex (**R**)) are presented in kcal/mol (see Supporting Materials for full structure parameters, as well as for the structures for the methanol formation pathway). Same color code as Fig. 1. (For interpretation of the references to colour in this figure legend, the reader is referred to the web version of this article.)

calculations show that *prior to* the protonation of methoxy or phenoxy ligands, intermediate (**P2a**) must undergo a Berry pseudorotation that locates the leaving group in an axial site of the trigonal bipyramid. This process occurs through transition state **TS2a** and leads to intermediate **P3a**. It requires a 22.0/22.3 and 19.3/20.3 kcal/mol energy barrier and is uphill by 10.2/11.9 and 12.8/13.5 kcal/mol for the pathways leading to the methanol (M) and phenol (P) formation, respectively. For example, as seen in Figs. 6 and 7, at the transition state (**TS2a**) leading to the phenol formation, the Zr-O^2H(P) bond is elongated from 2.251 to 2.375 Å, but the Zr-O^1(P) bond is shortened (from 2.239 to 2.141 Å), compared to their values in intermediate (**P2a**). Overcoming this transition state leads to cleavage of Zr-O^2H(P) bond: in intermediate (**P2a**) it is calculated to be 3.886 Å.

Close analyses show that the protonation of the methoxy or phenoxy ligands of the phosphorus intermediate **P3a** may proceed via multiple pathways. Herein, we identified two of them designated as "*internal*" and "*external*" protonation pathways. In the first case, the O^2H-ligand of the phosphate acts as a proton source, while in the latter case, the required proton comes from the Zr-coordinated water molecule. Since among these two pathways, the "*external*" protonation (i.e. by the Zr-coordinated water molecule) is kinetically less demanding and requires insignificant (> 1 kcal/mol) energy barriers (at the transition state (**TS_elim**), see Fig. 8), calculated relative to the corresponding isomer of the intermediate (**P3a**), below we only briefly discuss the "*external*" protonation pathway (transition states and products of the "*internal*" protonation pathway are given in the Supporting Materials).

Since the transition states (**TS_elim**) (see Fig. 8, as well as supporting materials) are lower in energy than the corresponding Berry pseudorotation transition state (**TS2a**), they are not expected to be rate-determining and will not impact the outcome of overall decomposition reaction. Thus, the Berry pseudorotation is the rate-limiting step of the DMPP decomposition by ZrPOM proceeding via the "*OH-transfer first*" and followed by the "*external*" protonation mechanism (below, we will call this mechanism of overall reaction just "*OH-transfer first*" mechanism). Furthermore, if the reaction proceeds via this mechanism then one should expect mostly phenol and (*O,O*-dimethyl)-(*O*-hydrogen)-phosphate (DMHP) as the DMPP decomposition products.

Thus, the above presented findings clearly show that from the two possible mechanisms of DMPP decomposition by the ZrPOM, i.e. "*hydrolysis first*" and "*OH-transfer first*", the "*OH-transfer first*" pathway requires a smaller rate-limiting energy barrier, 19.3/20.3 kcal/mol (for the Berry pseudorotation) *vs* 29.5/30.1 kcal/mol for the "*hydrolysis first*" mechanism. In other words, the presence of a hydroxo ligand in the coordination sphere of Zr(IV) elicits a mechanistic switch from "*hydrolysis first*" (previously reported [64] for the Sarin (GB) decomposition by the hexaniobate POM $Cs_8Nb_6O_{19}$) to "*OH-transfer first*". These findings imply that pH change of the catalytic solution, and therefore the hydroxide concentration, could be one of the mechanism controlling factors of the nerve agent and simulant decomposition by polyoxometalates.

3.1. Para-nitro-substitution effect on the mechanism of methyl-paraoxon (DMNP) decomposition by ZrPOM

While the calculated rate-limiting barriers of the DMPP decomposition by the ZrPOM are accessible at room temperature, the above presented discussion and discovered "phenoxy dissociation-then-proton-abstraction" nature of the rate-limiting transition state of the "*hydrolysis first*" pathway indicate that the presence of a strong electron-withdrawing *para*-substituent in the phenyl group could further reduce the rate-limiting energy barrier of this reaction. In order to validate this prediction, we now briefly discuss the mechanism of the (*O,O*-dimethyl)-(*O*-4-nitrophenyl)-phosphate (DMNP) decomposition by ZrPOM, which only differs from DMPP in the *para*-nitro substituent. We have investigated both the "*hydrolysis first*" and "*OH-transfer first*" pathways, which we discuss very briefly.

Extensive calculations (see Supporting Materials) of the first step of the *OH-transfer first* mechanism, i.e. (*para*-**R**) → (*para*-**TS1a**) → (*para*-**P2a**), for DMNP (the simulant with the *para*-nitro substituted phenyl) and comparison with those for DMPP (the simulant with a non-substituted phenyl group) show that *para*-nitro substitution has almost no impact on the calculated geometries and energetics of the associated transition state and intermediate. This process is endothermic by 5.0/6.6 kcal/mol (*vs* 5.9/5.8 kcal/mol) and proceeds over a reasonably low energy barrier (9.5/11.6 kcal/mol for DMNP and 11.3/12.3 kcal/mol for DMPP) (see Fig. 8). However, as anticipated, *para*-nitro substitution to phenyl has a strong impact on the calculated relative energy of the rate-limiting Berry pseudorotation transition state (*para*-**TS2a**) and reduces it from 19.3/20.3 kcal/mol (for DMPP) to 15.1/15.8 kcal/mol (for DMNP). Thus, indeed, the presence of strong electron-withdrawing *para*-nitro substitution in DMNP makes its decomposition by ZrPOM more facile.

Briefly, our findings (see Supporting Materials) for the DMNP decomposition by ZrPOM via the "*hydrolysis first*" mechanism show that introducing a strong electron-withdrawing *para*-nitro-substituent to phenyl, i.e. converting of DMPP to DMNP, (a) reduces the rate-limiting phenol formation energy barrier from 29.5/30.1 kcal/mol (for DMPP) to 19.8/21.8 kcal/mol (for DMNP), and (b) makes the phenol and (*O,O*-dimethyl)-(*O*-hydrogen)-phosphate (DMHP) formation thermodynamically even more accessible. Since the "*hydrolysis-first*" mechanism is, as previously was reported [64], the main decomposition

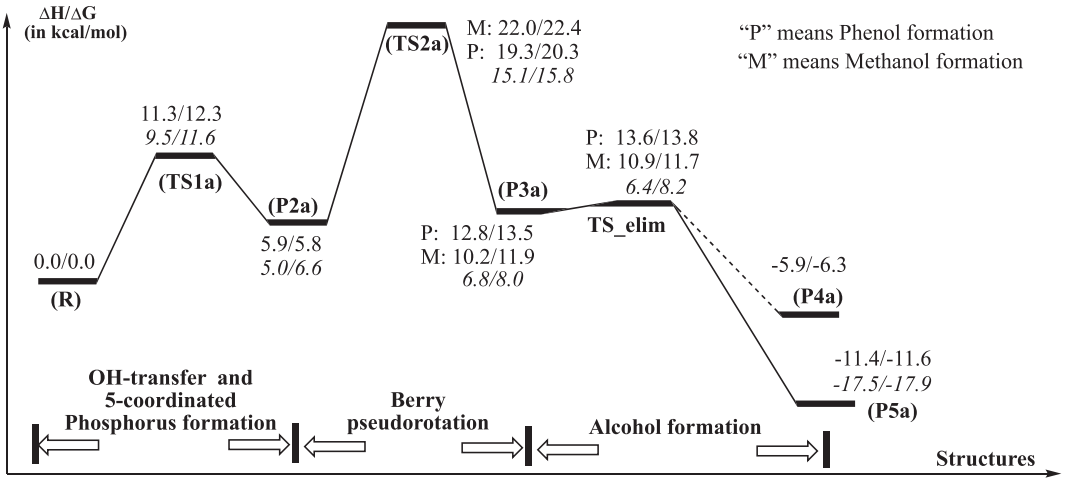

Fig. 8. The calculated OH-transfer transition state (**TS1a**) and intermediate (**P2a**). Selected bond distances of these structures are given in Å, while their relative energies (relative to pre-reaction complex (**R**)) are presented in kcal/mol (see Supporting Materials for full structure parameters). Same color code as Fig. 1. (For interpretation of the references to colour in this figure legend, the reader is referred to the web version of this article.)

mechanism of Sarin (GB) by the Lindqvist hexaniobate salts (for example, $Cs_8Nb_6O_{19}$), this critical role of *para*-nitro-substitution to phenyl is also expected to be valid for the case of DMPP and DMNP decomposition by the hexaniobate salts.

4. Conclusions

We have reported an extensive DFT study of the mechanism and controlling factors of (*O,O*-dimethyl)-(*O*-4-nitrophenyl)-phosphate (DMNP) and (*O,O*-dimethyl)-(*O*-phenyl)-phosphate (DMPP) decomposition by the zirconium-substituted polyoxometalate, $\{\alpha\text{-}PW_{11}O_{39}Zr(\mu\text{-}OH)(H_2O)\}^{4-}$, ZrPOM. We studied two mechanisms described as "*hydrolysis first*" and "*OH-transfer first*". The "*hydrolysis first*" mechanism is initiated from a pre-reaction complex (H_2O)-(OH)-POM-(nerve agent) and proceeds via the: (a) concerted dissociation of the adsorbed water molecule on a basic oxygen atom of the POM and nucleophilic addition of the nascent OH group to the phosphorus atom of the nerve agent, (b) rapid reorganization of the resulting pentacoordinated phosphorus intermediate, and (c) dissociation of the decomposition products and regeneration of the catalyst. The "*OH-transfer first*" mechanism is also initiated from the same pre-reaction complex (H_2O)-(OH)-POM-(nerve agent) but proceeds via the: (a) OH-ligand transfer from zirconium to the phosphorus of the nerve agent simulant and formation of the pentacoordinated phosphorus intermediate, (b) rate-limiting Berry pseudorotation, (c) protonation of the phenoxy group of the substrate by the Zr-coordinated water molecule, and (d) dissociation of the decomposition products [phenol and *O,O*-dimethyl)-(*O*-hydrogen)-phosphate (DMHP)] and regeneration of the catalyst.

Calculations show that the "*OH-transfer first*" pathway is the preferable mechanism for the decomposition of DMPP by ZrPOM. Thus, the presence of a hydroxo ligand in the coordination sphere of Zr(IV) introduces a mechanistic switch from "*hydrolysis first*" [which previously was reported [64] for the Sarin (GB) decomposition mechanism by the cesium salt of hexaniobate, $Cs_8Nb_6O_{19}$] to "*OH-transfer first*". These findings suggest that the pH of the catalytic solution might play a critical role and enable mechanism control of the nerve agent and simulant decomposition by polyoxometalates.

We predicted and corroborated that the presence of a strong electron-withdrawing *para*-substituent in the phenyl group of the substrate reduces the rate-limiting energy barrier of this reaction: the DMNP (with *para*-nitro-substituted phenyl) decomposition by ZrPOM occurs with smaller rate-limiting energy barrier than DMPP (the simulant with a non-substituted phenyl group), and leads to the *para*-nitro-phenol and DMHP as the decomposition products.

In summary, the calculations presented herein have revealed factors facilitating DMNP decomposition by Zr(IV)-substituted polyoxometalates. This knowledge renders Zr(IV)-substituted polyoxometalates attractive candidates for CWA decomposition. Furthermore, this class of POMs constitute a molecular and readily modifiable alternative to and analogue of Zr-containing MOFs (such as UiO-66, NU-1000 and MOF-808) and zirconium hydroxide, both extensively studied classes of compounds for organophosphorus nerve agent decomposition. We anticipate that these findings will be helpful in designing Zr-based materials that can catalytically decompose CWAs and other toxic compounds under ambient conditions.

Acknowledgements

This work is supported by the U.S. Army Research Laboratory and the U.S. Army Research Office under grant number W911NF-15-2-0107. The authors thank the Defense Threat Reduction Agency for support under program BB11PHM156. The authors acknowledge the Cherry L. Emerson Center for Scientific Computation at Emory University and Virginia Tech's Advanced Research Computing for providing computational resources.

Conflicts of interest

There are no conflicts to declare.

Appendix A. Supplementary data

Supplementary data to this article can be found online at https://doi.org/10.1016/j.chemphys.2018.11.013.

References

[1] L. Szinicz, Toxicology 214 (2005) 167.
[2] Y.-C. Yang, J.A. Baker, J.R. Ward, Chem. Rev. 92 (1992) 1729.
[3] M. Dixon, D.M. Needham, Nature 158 (1946) 432.
[4] K. Kim, O.G. Tsay, D.A. Atwood, D.G. Churchill, Chem. Rev. 111 (2011) 5345.
[5] (a) F.M. Raushel, Nature 469 (2011) 310;
(b) M. Enserink, Science 341 (2013) 1050.
[6] N. Sharma, R. Kakkar, Adv. Mat. Lett. 4 (2013) 508.
[7] R.H. Pastel, E.C. Ritchie, Psychological Responses to the New Terrorism: A NATO-Russia Dialogue, IOS Press, Amsterdam, 2005, pp. 9–24.
[8] Y.J. Yang, K. Kim, O.G. Tsay, D.A. Atwood, D.G. Churchill, Chem. Rev. 115 (2015) PR1.
[9] J.B. DeCoste, G.W. Peterson, Chem. Rev. 114 (2014) 5695.
[10] H. Stone, D. See, A. Smiley, A. Ellingson, J. Schimmoeller, L. Oudejans, J. Hazard. Mater. 314 (2016) 59.

[11] G.K. Prasad, P. Ramacharyulu, B. Singh, J. Sci. Ind. Res. 70 (2011) 91.
[12] G.W. Wagner, Ind. Eng. Chem. Res. 50 (2011) 12285.
[13] S.S. Talmage, A.P. Watson, V. Hauschild, N.B. Munro, J. King, Current Org. Chem. 11 (2007) 285.
[14] (a) J.L. Sussman, M. Harel, F. Frolow, C. Oefner, A. Goldman, L. Toker, I. Silman, Science 253 (1991) 872;
(b) A. Tripathi, Ann. Neurosci. 15 (2008) 106.
[15] S.Y. Moon, G.W. Wagner, J.E. Mondloch, G.W. Peterson, J.B. DeCoste, J.T. Hupp, O.K. Farha, Inorg. Chem. 54 (2015) 10829.
[16] C. Montoro, F. Linares, E.Q. Procopio, I. Senkovska, S. Kaskel, S. Galli, N. Masciocchi, E. Barea, J.A.R. Navarro, J. Am. Chem. Soc. 133 (2011) 11888.
[17] M.J. Katz, J.E. Mondloch, R.K. Totten, J.K. Park, S.T. Nguyen, O.K. Farha, J.T. Hupp, Angew. Chem. Int. Ed. 53 (2014) 497.
[18] P. Li, R.C. Klet, S.-Y. Moon, T.C. Wang, P. Deria, A.W. Peters, B.M. Klahr, H.-J. Park, S.S. Al-Juaid, J.T. Hupp, O.K. Farha, Chem. Commun. 51 (2015) 10925.
[19] Y. Liu, S.Y. Moon, J.T. Hupp, O.K. Farha, ACS Nano 9 (2015) 12358.
[20] J.E. Mondloch, M.J. Katz, W.C. Isley, P. Ghosh, P.L. Liao, W. Bury, W.G. Wagner, M.G. Hall, J.B. DeCoste, G.W. Peterson, R.Q. Snurr, C.J. Cramer, J.T. Hupp, O.K. Farha, Nature Mater. 14 (2015) 512.
[21] S.Y. Moon, Y. Liu, J.T. Hupp, O.K. Farha, Angew. Chem. Int. Ed. 54 (2015) 6795.
[22] E. Lopez-Maya, C. Montoro, L.M. Rodriguez-Albelo, S.D.A. Cervantes, A.A. Lozano-Perez, J.L. Cenis, E. Barea, J.A.R. Navarro, Angew. Chem. Int. Ed. 54 (2015) 6790.
[23] S.S. Mondal, H.J. Holdt, Angew. Chem. Int. Ed. 55 (2016) 42.
[24] G. Wang, C. Sharp, A.M. Plonka, Q. Wang, A.I. Frenkel, W. Guo, C. Hill, C. Smith, J. Kollar, D. Troya, J.R. Morris, J. Phys. Chem. C 121 (2017) 11261.
[25] A.M. Plonka, Q. Wang, W.O. Gordon, A. Balboa, D. Troya, W. Guo, C.H. Sharp, S.D. Senanayake, J.R. Morris, C.L. Hill, A.I. Frenkel, J. Am. Chem. Soc. 139 (2017) 599.
[26] S.Y. Moon, E. Proussaloglou, G.W. Peterson, J.B. DeCoste, M.G. Hall, A.J. Howarth, J.T. Hupp, O.K. Farha, Chem. A, Eur. J. 22 (2016) 14864.
[27] S.-Y. Moon, A.J. Howarth, T. Wang, N.A. Vermeulen, J.T. Hupp, O.K. Farha, Chem. Commun. 52 (2016) 3438.
[28] R. Gaillac, P. Pulumbi, K.A. Beyer, K.W. Chapman, D.A. Keen, T.D. Bennet, F.X. Coudert, Nat. Mater. 16 (2017) 1149.
[29] (a) D. Yang, V. Bernales, T. Islamoglu, O.K. Farha, J.T. Hupp, C.J. Cramer, L. Gagliardi, B.C. Gates, J. Am. Chem. Soc. 138 (2016) 15189;
(b) D. Yang, M.A. Ortuño, V. Bernales, C.J. Cramer, L. Gagliardi, B.C. Gates, J. Am. Chem. Soc. 140 (2018) 3751.
[30] T. Islamoglu, A. Atilgan, S.-Y. Moon, G.W. Peterson, J.B. DeCoste, M. Hall, J.T. Hupp, O.K. Farha, Chem. Mater. 29 (2017) 2672.
[31] Q. Wang, R.C. Chapleski Jr., A.M. Plonka, W.O. Gordon, W. Guo, T.D. Nguyen-Phan, C.H. Sharp, N.S. Marinkovic, S.D. Senanayake, J.R. Morris, C.L. Hill, D. Troya, A.I. Frenkel, Sci. Rep. 7 (2017) 773.
[32] D.M. Mizrahi, S. Saphier, I. Columbus, J. Hazard. Mater. 179 (2010) 495.
[33] W. Guo, H. Lv, K.P. Sullivan, W.O. Gordon, A. Balboa, G.W. Wagner, D.G. Musaev, J. Bacsa, C.L. Hill, Angew. Chem. Int. Ed. 55 (2016) 7403.
[34] M.K. Kinnan, W.R. Creasy, L.B. Fullmer, H.L. Schreuder-Gibson, M. Nyman, Eur. J. of Inorg. Chem. 2014 (2014) 2361.
[35] (a) N.M. Okun, J.C. Tarr, D.A. Hilleshiem, L. Zhang, K.I. Hardcastle, C.L. Hill, J. Mol. Catal. A. Chem. 246 (2006) 11;
(b) N.M. Okun, T.M. Anderson, C.L. Hill, J. Mol. Catal. A: Chem. 197 (2003) 283;
(c) F. Carniato, C. Bisio, R. Psaro, L. Marchese, M. Guidotti, Angew. Chem. Int. Ed. 53 (2014) 10095.
[36] J. Song, Z. Luo, D.K. Britt, H. Furukawa, O.M. Yaghi, K.I. Hardcastle, C.L. Hill, J. Am. Chem. Soc. 133 (2011) 16839.
[37] F.J. Ma, S.X. Liu, C.Y. Sun, D.D. Liang, G.J. Ren, F. Wei, Y.G. Chen, Z.M. Su, J. Am. Chem. Soc. 133 (2011) 4178.
[38] M. Carraro, S. Gross, Materials 7 (2014) 3956.
[39] A. Proust, B. Matt, R. Villanneau, G. Guillemot, P. Gouzerh, G. Izzet, Chem. Soc. Rev. 41 (2012) 7605.
[40] T.J. Bandosz, M. Laskoski, J. Mahle, G. Mogilevsky, G.W. Peterson, J.A. Rossin, G.W. Wagner, J. Phys. Chem. C 116 (2012) 11606.
[41] R.B. Balow, J.G. Lundin, G.C. Daniels, W.O. Gordon, M. McEntee, G.W. Peterson, J.H. Wynne, P.E. Pehrsson, ACS Appl. Mater. Interfaces 9 (2017) 39747.
[42] S.W. Yang, D.C. Doetschman, J.T. Schulte, J.B. Sarnbur, C.W. Kanyi, J.D. Fox, Microporous Mesoporous Mater. 92 (2006) 56.
[43] S.M. Kanan, C.P. Tripp, Langmuir 17 (2001) 2213.
[44] L. Bromberg, H. Schreuder-Gibson, W.R. Creasy, D.J. McGarvey, R.A. Fry, T.A. Hatton, Ind. and Eng. Chem. Res. 48 (2009) 1650.
[45] G.W. Wagner, Q. Chen, Y. Wu, J. Phys. Chem. C 112 (2008) 11901.
[46] G.W. Wagner, G.W. Peterson, J.J. Mahle, Ind. Eng. Chem. Res. 51 (2012) 3598.
[47] G.W. Wagner, L.R. Procell, R.J. O'Conner, S. Munavalli, C.L. Carnes, P.N. Kapoor, K.J. Klabunde, J. Am. Chem. Soc. 123 (2001) 1636.
[48] (a) T. Yamase, M.T. Pope, Nanostructure Science and Technology, Kluwer Academic/Plenum Publishers, New York, 2002;
(b) M.T. Pope, Comprehensive Coordination Chemistry II: From Biology to Nanotechnology, Elsevier Ltd., Oxford, UK, 2004, pp. 635–678;
(c) H.N. Miras, J. Yan, D.-L. Long, L. Cronin, Chem. Soc. Rev. 41 (2012) 7403;
(d) H. Lv, Y.V. Geletii, C. Zhao, J.W. Vickers, G. Zhu, Z. Luo, J. Song, T. Lian, D.G. Musaev, C.L. Hill, Chem. Soc. Rev. 41 (2012) 7572.
[49] (a) As an example for computational studies of the POMs see: J.M. Poblet, X. Lopez, C. Bo, Chem. Soc. Rev. 32 (2003) 297;
(b) P. Miro, J.M. Poblet, J.B. Avalos, C. Bo, Can. J. Chem. 87 (2009) 1296;
(c) C. Bo, J.M. Poblet, Israel J. Chem. 51 (2011) 228;
(d) X. Lopez, P. Miro, J.J. Carbo, A. Rodriguez-Fortea, C. Bo, J.M. Poblet, Theor. Chem. Acc. 128 (2011) 393;
(e) X. Lopez, J.J. Carbo, C. Bo, J.M. Poblet, Chem. Soc. Rev. 41 (2012) 7537;
(f) B. Matt, X. Xiang, A.L. Kaledin, N.N. Han, J. Moussa, H. Amouri, S. Alves, C.L. Hill, T.Q. Lian, D.G. Musaev, G. Izzet, A. Proust, Chem. Sci. 4 (2013) 1737;
(g) A.E. Kuznetsov, Y.V. Geletii, C.L. Hill, K. Morokuma, D.C. Musaev, J. Am. Chem. Soc. 131 (2009) 6844.
[50] S.-S. Wang, G.-Y. Yang, Chem. Rev. 115 (2015) 4893.
[51] C.L. Hill, J. Mol. Cat. A: Chem. 262 (2007) 2.
[52] D.L. Long, R. Tsunashima, L. Cronin, Angew. Chem. Int. Ed. 49 (2010) 1736.
[53] H. Stephan, M. Kubeil, F. Emmerling, C.E. Müller, Eur. J. Inorg. Chem. 2013 (2013) 1585.
[54] N.V. Izarova, M.T. Pope, U. Kortz, Angew. Chem. Int. Ed. 51 (2012) 9492.
[55] C. Boglio, G. Lemiere, B. Hasenknopf, S. Thorimbert, E. Lacote, M. Malacria, Angew. Chem. Int. Ed. 45 (2006) 3324.
[56] O.A. Kholdeeva, G.M. Maksimov, R.I. Maksimovskaya, M.P. Vanina, T.A. Trubitsina, D.Yu. Naumov, B.A. Kolesov, N.S. Antonova, J.J. Carbo, J.M. Poblet, Inorg. Chem. 45 (2006) 7224.
[57] C.N. Kato, A. Shinohara, K. Hayashi, K. Nomiya, Inorg. Chem. 45 (2006) 8108.
[58] B.S. Bassil, M.H. Dickman, U. Kortz, Inorg. Chem. 45 (2006) 2394.
[59] H. Carabineiro, R. Villanneau, X. Carrier, P. Herson, F. Lemos, F. Ramôa Ribeiro, A. Proust, M. Che, Inorg. Chem. 45 (2006) 1915.
[60] I.A. Weinstock, R.E. Schreiber, R. Neumann, Chem. Rev. 118 (2017) 2680.
[61] J. Li, R. Güttinger, R. Moré, F. Song, W. Wan, G.R. Patzke, Chem. Soc. Rev. 46 (2017) 6124.
[62] (a) M.R. Antonio, M. Nyman, T.M. Anderson, Angew. Chem. Int. Ed. 121 (2009) 6252;
(b) M. Nyman, T.M. Alam, F. Bonhomme, M.A. Rodriguez, C.S. Frazer, M.E. Welk, J. Cluster Sci. 17 (2006) 197;
(c) M. Nyman, Dalton Trans. 40 (2011) 8049;
(d) E.M. Villa, C.A. Ohlin, E. Balogh, T.M. Anderson, M.D. Nyman, W.H. Casey, Angew. Chem. Int. Ed. 47 (2008) 4844;
(e) E. Balogh, T.M. Anderson, J.R. Rustad, M. Nyman, W.H. Casey, Inorg. Chem. 46 (2007) 7032.
[63] M. Nyman, F. Bonhomme, T.M. Alam, M.A. Rodriguez, B.R. Cherry, J.L. Krumhansl, T.M. Nenoff, A.M. Sattler, Science 297 (2002) 996.
[64] R.C. Chapleski Jr., D.G. Musaev, C.L. Hill, D. Troya, J. Phys. Chem. C 120 (2016) 16822.
[65] A.L. Kaledin, D.M. Driscoll, D. Troya, D. Collins-Wildman, C.L. Hill, J.R. Morris, D.G. Musaev, Chem. Sci. 9 (2018) 2147.
[66] K. Nomiya, Y. Saku, S. Yamada, W. Takahashi, H. Sekiya, A. Shinohara, M. Ishimaru, Y. Sakai, Dalton Trans. (2009) 5504.
[67] H.G.T. Ly, G. Absillis, T.N. Parac-Vogt, Dalton Trans. 42 (2013) 10929.
[68] T.K.N. Luong, G. Absillis, P. Shestakova, T.N. Parac-Vogt, Eur. J. Inorg. Chem. 2014 (2014) 5276.
[69] T.K.N. Luong, G. Absillis, P. Shestakova, T.N. Parac-Vogt, Dalton Trans. 44 (2015) 15690.
[70] T.K.N. Luong, P. Shestakova, T.T. Mihaylov, G. Absillis, K. Pierloot, T.N. Parac-Vogt, Chem. A, Eur. J. 21 (2015) 4428.
[71] T.K.N. Luong, P. Shestakova, G. Absillis, T.N. Parac-Vogt, Inorg. Chem. 55 (2016) 4864.
[72] T.T. Mihaylov, H.G.T. Ly, K. Pierloot, T.N. Parac-Vogt, Inorg. Chem. 55 (2016) 9316.
[73] S. Vanhaecht, G. Absillis, T.N. Parac-Vogt, Dalton Trans. 41 (2012) 10028.
[74] G. Absillis, T.N. Parac-Vogt, Inorg. Chem. 51 (2012) 9902.
[75] T.K.N. Luong, P. Shestakova, T.N. Parac-Vogt, Dalton Trans. 45 (2016) 12174.
[76] H.G.T. Ly, T. Mihaylov, G. Absillis, K. Pierloot, T.N. Parac-Vogt, Inorg. Chem. 54 (2015) 11477.
[77] H.G.T. Ly, G. Absillis, S.R. Bajpe, J.A. Martens, T.N. Parac-Vogt, Eur. J. Inorg. Chem. 2013 (2013) 4601.
[78] Y. Tian, A.M. Plonka, A.M. Ebrahim, R.M. Palomino, S.D. Senanayake, A. Balboa, W.O. Gordon, D. Troya, D.G. Musaev, J.R. Morris, M.B. Mitchell, D.L. Collins-Wildman, C.L. Hill, A.I. Frenkel, Sci. Rev. Adv. (2018).
[79] D.L. Collins-Wildman, M. Kim, K.P. Sullivan, A.M. Plonka, A.I. Frenkel, D.G. Musaev, C.L. Hill, ACS Catal. 8 (2018) 7068.
[80] M.J. Frisch, G.W. Trucks, H.B. Schlegel, G.E. Scuseria, M.A. Robb, J.R. Cheeseman, G. Scalmani, V. Barone, B. Mennucci, G.A. Petersson, H. Nakatsuji, M. Caricato, X. Li, H.P Hratchian, A.F. Izmaylov, J. Bloino, G. Zheng, J.L. Sonnenberg, M. Hada, M. Ehara, K. Toyota, R. Fukuda, J. Hasegawa, M. Ishida, T. Nakajima, Y. Honda, O. Kitao, H. Nakai, T Vreven, J.A. Montgomery, Jr., J.E. Peralta, F.ß. Ogliaro, M.J. Bearpark, J. Heyd, E.N. Brothers, K.N. Kudin, V.N. Staroverov, R. Kobayashi, J. Normand, K. Raghavachari, A.P. Rendell, J.C. Burant, S.S. Iyengar, J. Tomasi, M. Cossi, N. Rega, N.J. Millam, M. Klene, J.E. Knox, J.B. Cross, V. Bakken, C. Adamo, J. Jaramillo, R. Gomperts, R.E. Stratmann, O. Yazyev, A.J. Austin, R. Cammi, C. Pomelli, J.W. Ochterski, R.L. Martin, K. Morokuma, V.G. Zakrzewski, G.A. Voth, P. Salvador, J.J. Dannenberg, A. Dapprich, A.D. Daniels, Ö. Farkas, J.B. Foresman, J.V. Ortiz, J. Cioslowski, D.J. Fox, Gaussian, Inc.: Wallingford, CT, USA, 2009.
[81] Y. Zhao, D.G. Truhlar, J. Chem. Phys. 125 (2006) 194101.
[82] (a) E. Cances, B. Mennucci, J. Tomasi, J. Chem. Phys. 107 (1997) 3032;
(b) B. Mennucci, J. Tomasi, J. Chem. Phys. 106 (1997) 5151;
(c) G. Scalmani, M.J. Frisch, J. Chem. Phys. 132 (2010) 114110.